



Article

Experimental Evaluation of a Photovoltaic/Thermal Air Heater with Metal Mesh-Integrated Thermal Energy Storage System

Azim Doğuř Tuncer ¹, Emine Yađız Gurbüz ², Ali Keeabař ² and Aleksandar G. Georgiev ^{3,*}

¹ Department of Energy Systems Engineering, Faculty of Engineering-Architecture, Burdur Mehmet Akif Ersoy University, 15030 Burdur, Turkey; azimdtuncer@gmail.com

² Department of Energy Systems Engineering, Technology Faculty, Muđla Sıtkı Koman University, 48000 Muđla, Turkey; eminegurbuz@mu.edu.tr (E.Y.G.); alikecebas@mu.edu.tr (A.K.)

³ Department of General Engineering, University of Telecommunications and Posts, 1 Akad. Stefan Mladenov Str., 1700 Sofia, Bulgaria

* Correspondence: ageorgiev@gmx.de

Abstract: The objective of this study is to improve the performance of a hybrid photovoltaic/thermal (PV/T) air heater incorporating a thermal energy storage system (TESS) that uses paraffin and has metallic mesh layers. In the experimental part of the research, three different pilot-scale PV/Ts have been designed, manufactured, and experimentally investigated. The first system was structured as a conventional PV/T, while the second (PVT/TESS) was modified with a paraffin-based TESS. The efficiency of a hybrid PV/T air heater was improved by integrating a paraffin-based thermal energy storage system (TESS) with metallic mesh layers (PV/T-MTESS). The performance of the modified PV/T-MTESS system was compared to two other PV/T systems under the same weather conditions and air flow rate. The results of the experiment demonstrated that the integration of mesh layers into the TESS led to substantial improvements in the system's thermal and electrical performance, as well as its overall exergy efficiency. The improvements were 33.17%, 14.82%, and 58.15%, respectively, when compared to the unaltered (conventional) PV/T setup. Moreover, an enviro-economic analysis has been performed on the developed and tested PV/Ts. Using TESS with only paraffin and with mesh layer-added paraffin reduced the payback time of the system by 2.54% and 9.85%, respectively. Moreover, the annual carbon dioxide saving was improved from 0.079 tons/year to 0.103 tons/year using a mesh layer-integrated TESS in the PV/T air heater.

Keywords: photovoltaic/thermal; solar air heater; thermal energy storage; metal meshes



Citation: Tuncer, A.D.; Gurbüz, E.Y.; Keeabař, A.; Georgiev, A.G.

Experimental Evaluation of a Photovoltaic/Thermal Air Heater with Metal Mesh-Integrated Thermal Energy Storage System. *Energies* **2023**, *16*, 3449. <https://doi.org/10.3390/en16083449>

Academic Editor: Carlo Renno

Received: 18 March 2023

Revised: 7 April 2023

Accepted: 11 April 2023

Published: 14 April 2023



Copyright: © 2023 by the authors. Licensee MDPI, Basel, Switzerland. This article is an open access article distributed under the terms and conditions of the Creative Commons Attribution (CC BY) license (<https://creativecommons.org/licenses/by/4.0/>).

1. Introduction

Human activities have led to the excessive utilization of fossil fuel-based energy technologies, resulting in global warming and environmental pollution [1]. The use of renewable energy sources, particularly solar energy, can help mitigate carbon pollution [2]. Solar energy, which is the fastest-growing renewable source, has several advantages in terms of applicability compared to other renewable sources. Various solar collectors [3], photovoltaic (PV) cells [4], and photovoltaic/thermal (PV/T) hybrid solar air heaters [5] are commonly used for solar energy conversion. PV and PV/T systems can be installed in unique locations such as mountains, seas, and deserts unlike other alternative energy sources [6]. The solar industry has expanded globally, resulting in reduced manufacturing costs and improved performance rates of solar systems. As a result, scientists and experts have been exploring ways to improve the effectiveness of PV and PV/T systems [7,8]. Numerous studies have examined the reduction in system performance that is caused by the increase in temperature on the surface of the panel. To address this issue, scholars have explored passive cooling methods, hybrid energy systems (both electrical and thermal), and heat storage systems in academic research [4,9]. The PV system generates electricity by activating the electricity generation mechanism using the sun's rays. However, several

factors such as temperature, radiation, shading, dust, and losses can affect the energy obtained from the PV system, thereby limiting the performance of PV cells, and releasing some of the energy as heat into the atmosphere [10]. To utilize unused energy, it is preferable to employ PV/T systems instead of PV cells. PV/T systems transform solar radiation into electrical energy via solar cells that are thermally linked to the absorbing surface. The surplus heat generated by the solar cells serves as the input heat for the thermal system, which is removed from the panel during operation. Cooling the panel in this manner can enhance the efficiency of the PV/T system [11]. Therefore, numerous studies have been conducted to investigate the performance of PV/T systems and develop diverse approaches. As an example, previous studies have explored different ways to improve the performance of PV/T systems. Kumar and Rosen [12] demonstrated that extending the fin area of a double-pass PV/T system with vertical fins in the bottom channel can reduce the temperature of PV cells from 82 °C to 66 °C. Othman et al. [13] conducted an experiment on a PV/T system that utilized water and air as cooling fluids and generated waste heat to heat water. The study found a 17% efficiency in electricity generation and a 76% efficiency in heat generation. In their study, Mourshed et al. [14] analyzed a hybrid PV/T system utilizing both air and water for cooling and observed that the system's efficiency was significantly influenced by variations in solar radiation and refrigerant flow rate. Recent research on PV/T systems has focused on improving their performance by designing and integrating various additions. For instance, Vassiliades et al. [15] used dynamic simulations to assess how well PV/T systems with hybrid technology performed in an eco-friendly prefabricated house located in various regions. Meanwhile, Kang et al. [16] utilized numerical analysis to investigate variations in efficiency between single-inlet air-cooled PV/T and multiple-input air-cooled PV/T systems. Gopi and Muraleedharan [17] discovered that an improved PV/T system outperformed a standard PV/T system in their study. Shahsavar and Arıcı [18] examined the performance of photovoltaic/thermal-wheel and photovoltaic/thermal-heat pipe-thermal wheel systems and found that the former had a 2.1% increase in energy output compared to the latter. Finally, Roshdan et al. [19] created a mathematical model and conducted experiments to assess the effectiveness of a compound parabolic concentrator designed for use on building facades, featuring an asymmetric shape.

The utilization of phase change materials (PCMs) in thermal regulation and solar energy systems including solar air heaters [20], hybrid PV/T systems [21,22], solar dryers [23,24], and solar stills [25] has been consistently increasing over time. The demand for energy-efficient products with low environmental impact has become a significant concern in recent years, which has led to the development of latent thermal energy storage systems (TESS) as a potential solution. Thermal energy storage (TES) finds applications in various fields, as highlighted in studies by Browne et al. [26] and Yang et al. [27]. While Selimefendigil et al. [28] analyzed the discharge performance of a cylindrical container containing PCMs with respect to variations in heat transfer fluids and geometry, Sopian et al. [29] compared the energy, exergy, and efficiency of various designs of hybrid PV/T systems. The study found that the PV/T with nanofluids and nano-PCM had the highest thermal efficiency, thermal energy, and electrical exergy, outperforming the conventional PV module. Behzadi and Arabkoohsar [30] proposed a "smart building energy system" that utilizes solar PV/T panels and a heat storage tank to supply heat and electricity to buildings and generate hot water that can be sold to the local ultralow-temperature district heating grid. Yao et al. [31] explored the use of PV/T technology with built-in PCM heat storage and a heat pump evaporator for heating applications in high-altitude areas. The study showed that the system's heating coefficient of performance (COP) increases with solar radiation intensity, ambient temperature, and PV/T collector area, and decreases with wind speed. Finally, Mao et al. [32] developed an operation strategy for a combined cooling, heating, and power system that utilizes PV/T panels and TES. The proposed method uses the particle swarm optimization algorithm to optimize the system size, leading to improved economic and energetic benefits, as demonstrated in case studies. As seen

in the literature given in the article, paraffin-based TESS has been shown to effectively reduce energy consumption and improve the performance of various heating and cooling systems [33]. Studies demonstrate that paraffins have a high latent heat of fusion and can be formulated to have a range of melting points, making them versatile for use in different temperature ranges [34]. Additionally, paraffins are relatively low-cost, readily available, chemically stable, and non-toxic, which makes them a safer and more sustainable option for TES [9,35]. These advantages make paraffins an attractive option for a wide range of TES applications, including solar water heating systems, space heating and cooling systems, and residential buildings.

Solar air heaters (SAHs) are a popular and cost-effective option for heating air, but their thermal efficiency is limited by the poor thermal properties of the circulating air. To address this issue, researchers have explored the use of techniques such as fins and baffles to enhance heat transfer and induce turbulence. Additionally, studies by Kabeel et al. [36] and Sajawal et al. [37] have demonstrated the potential benefits of incorporating PCMs into SAHs to enhance their thermal performance. Kabeel et al. [36] compared the thermal performance of flat and v-corrugated plate SAHs with built-in PCMs, while Sajawal et al. [37] explored the use of double pass SAHs with PCMs contained in metallic finned tubes. Both studies reported a significant improvement in the efficiency and effectiveness of SAHs when using PCMs. Salih et al. [38] also conducted a study on the use of PCMs in SAHs to improve thermal performance. The system used rectangular capsules containing a paraffin wax-based PCM and was tested at various airflow speeds and solar irradiance intensities. Results showed a substantial increase in efficiency and temperature rise compared to a system without PCMs. Abuşka et al. [39] conducted a study to evaluate the thermal performance of SAHs utilizing PCMs, comparing those with and without honeycomb internal fin structures. The findings revealed that incorporating honeycomb reduced the charge-discharge time and increased the temperature by up to 8.8 °C at the PCM temperature. However, it slightly decreased the instantaneous-daily thermal efficiency. Furthermore, Dinesh et al. [40] found that incorporating organic PCMs in a baffled SAH improved its energy efficiency by 11.25%, while Farzan et al. [41] enhanced the performance of SAHs with PCMs by embedding the PCM in expanded metal meshes. The utilization of a metallic mesh in a PV/T air heating system can improve both thermal and electrical performance through a variety of mechanisms. The metallic mesh can act as a heat sink to regulate the temperature of the collector and increase the air flow rate, which enhances heat transfer and improves thermal performance. The metallic mesh also improves the electrical conductivity of the PV/T system, reducing electrical losses and further enhancing system performance. This approach resulted in higher heat gain and energy efficiency compared to commercial SAHs.

Figure 1 depicts the main stages of the current study. In this study, the objective is to improve the thermal and electrical efficiency of a PV/T air heating system by integrating a TESS equipped with metallic mesh layers and paraffin. Unlike previous studies, this work incorporates metallic meshes into a TES unit of an air-flowing PV/T system for the first time. Three different systems were designed, fabricated, and tested under identical environmental conditions to evaluate the effect of this new modification on performance. These systems included a conventional (unmodified) system, a PV/T system with only paraffin-based TESS, and a PV/T system with a TESS with integrated mesh layers and paraffin-containing. Experimental results were analyzed from energetic, exergetic, and enviro-economic perspectives. The major findings of this study are presented and future research directions are discussed.

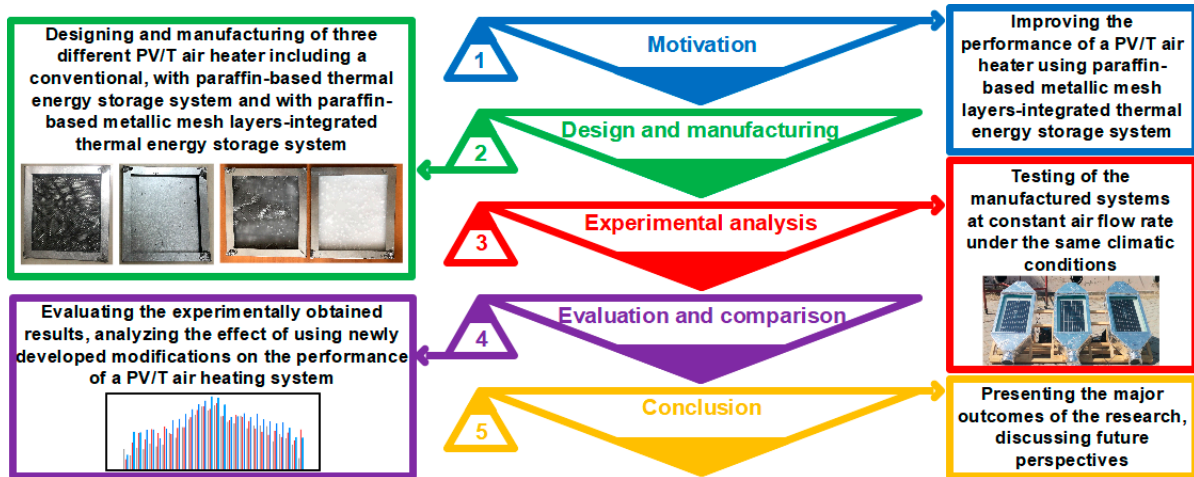


Figure 1. Main steps of the current study.

2. Materials and Methods

2.1. Test Setup

The objective of this study was to examine how the integration of a mesh-layer TESS affects the efficiency of a PV/T air heater. The TESS contained paraffin (brand: RUBITHERM, type: RT42) with a melting area of 38–43 °C and a specific heat capacity of 2 kJ/kgK, a thermal conductivity of 0.2 W/mK and a heat storage capacity of 165 kJ/kg. In addition, the volume expansion rate of the specific PCM was indicated as 12.5%. Two TESSs were created and tested: one with only paraffin and one with paraffin and metallic mesh layers. The metallic (steel) mesh layers had a thickness of 0.3 mm and the TESS basins were made of aluminum sheets with dimensions of 24 × 22 × 1.5 cm. Moreover, the thermal conductivity value of the steal meshes is ~45 W/mK. It should be noted that 85% of the manufactured basins were occupied with PCM and metallic meshes to prevent leakages. Figure 2 presents the preparation steps for the two TESS setups.

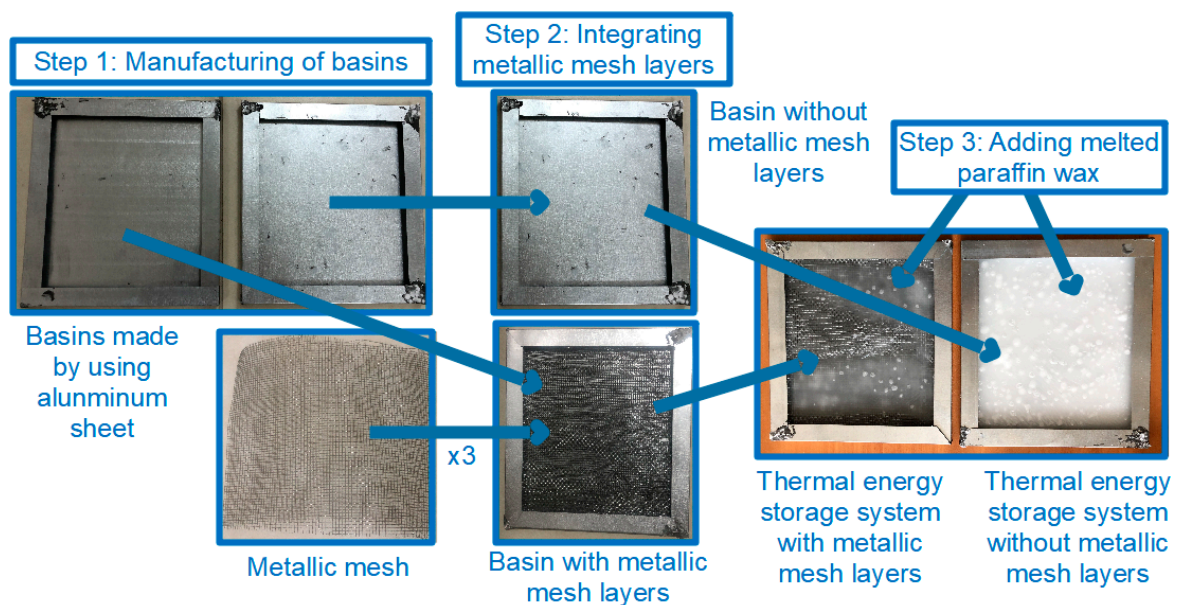


Figure 2. Photographic view of manufacturing steps of the two TESS setups.

The systems developed in this study utilized 12 monocrystalline PV modules manufactured by Solarinka with the model name 12 W Monoperc and dimensions of $36 \times 26 \times 2$ cm. The specifications of these modules are provided in Table 1. The TESS setups that were designed and fabricated were directly attached to the back (on the tedlar) of the PV modules using liquid seal and epoxy material. Three types of PV/T air heaters were manufactured in this work, all of which were designed as a parallel-flow air structure. In other words, the PV modules were positioned at the center of the air duct, allowing heat transfer via both sides of the PV module. The first system was a conventional parallel-flow PV/T system. The second PV/T (PV/T-TESS) incorporated a TESS containing only paraffin. The third PV/T system, named PV/T-MTESS, was modified to include the TESS with metallic mesh layers. The heater boxes were constructed using 2 cm-thick thermal insulation material, while 0.4 cm-thick glasses (transmissivity: 0.92) were used as transparent covers for all designed systems. Axial suction fans with dimensions of $7 \times 7 \times 1$ cm, powered by direct current, were also installed in each PV/T to provide air flow. It should be noted that PV panels in the PV/T systems were placed in the middle of the air channel to convey the heat from both surfaces of the PV panel with the flowing air. The depth of the air channels was 7 cm for all investigated systems. The dimensions of the developed PV/T systems are shown in Figure 3. While Figures 4 and 5 show a photograph and schematic illustration of the test setup, respectively.

Table 1. Details of the used photovoltaic modules.

Specification	Value
P_{max}	12 W
$I_{p,max}$	0.52 A
$V_{p,max}$	23.25 V
I_{sc}	0.58 A
V_{oc}	23.45 V

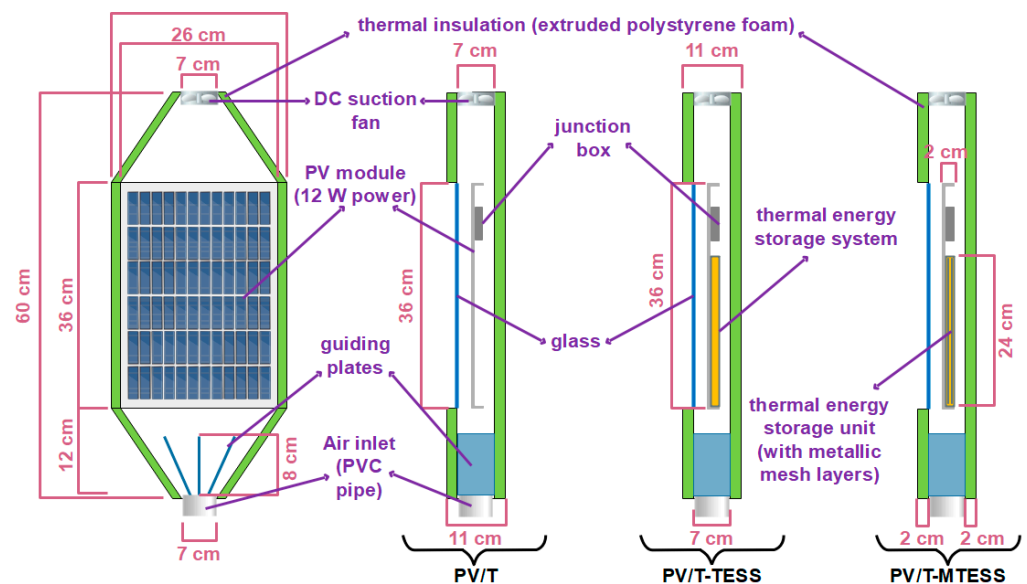


Figure 3. Dimensions and the components of the developed PV/T air heaters.

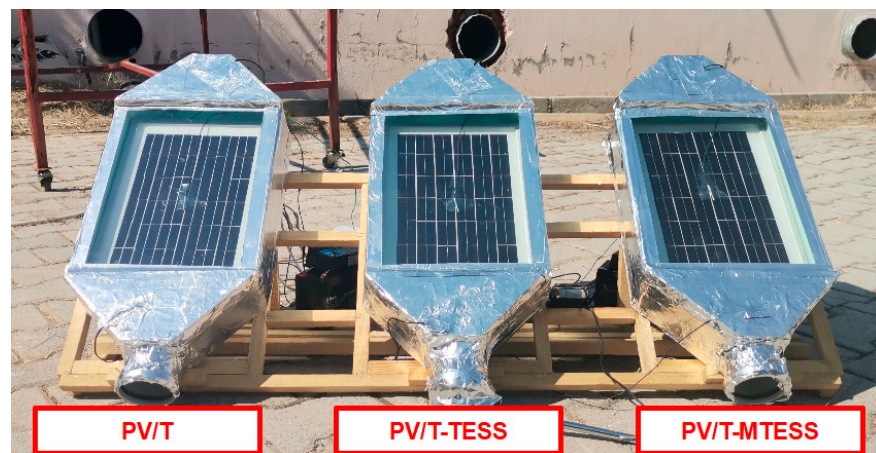


Figure 4. A photographic view of the experimental setup.

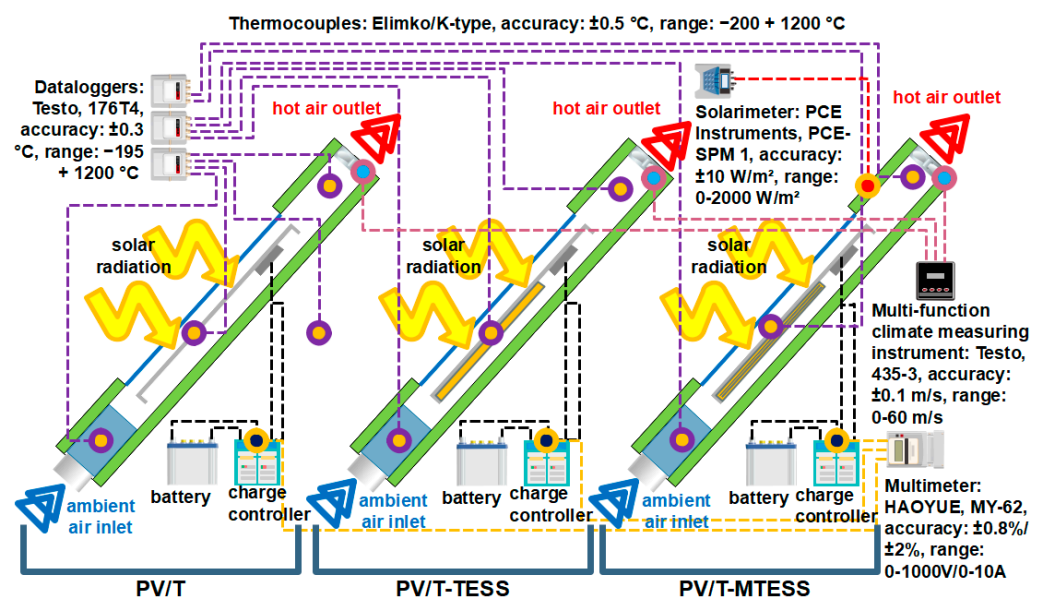


Figure 5. Schematic view of the experimental setup and utilized measurement devices.

2.2. Test Procedure

The experiment was conducted in July in the Muğla province of Turkey. The developed systems were tested simultaneously at a constant flow rate of 0.01 kg/s. Air velocity values in the systems were controlled using a special fan regulator. In the initial stage, analyzed systems that are covered with a fabric cover were taken to an outdoor environment. The utilized fans were operated for 15 min to ensure the airflow regime inside the systems was steady. At 9 AM, the fabric cover was removed and the experimental process was started. The experimental process ended at 6 PM. Temperature measurements were taken and recorded every 10 s, while other parameters such as radiation, air velocity, and electric voltage-current were measured and saved at 20 min intervals. The measurement devices used in the experiment are shown in Figure 5.

All three PV/T were tested simultaneously at the same conditions in order to make a good and reliable comparison between them. In this regard, the mass flow rate of the air was kept constant in the three systems. In the unmodified system, in order to obtain the same mass flow rate, the flow velocity was adjusted using fan regulators. In addition, the height of the PCM-filled container was 1 cm and did not have any important effect on the airflow inside the channel.

3. Theoretical Analysis

The energy balance in the PV/T air heating system can be written as [42]:

$$\sum \dot{E}_{inl} - \sum \dot{E}_{loss} = \sum \dot{E}_{out} \quad (1)$$

$$\dot{E}_{ma,inl} + \dot{E}_{sun} = \sum \dot{E}_{loss} + \dot{E}_{elec} + \dot{E}_{ma,out} \quad (2)$$

$$\dot{E}_{sun} = \dot{G}_{ef} \tau \alpha \quad (3)$$

It is worth noting that the effective solar radiation, represented by \dot{E}_{sun} , can be derived from the product of transmissivity, absorptivity, and overall solar irradiance (\dot{G}).

The absorbed heat from air in the PV/T is named useful thermal energy. This parameter can be found from:

$$\dot{E}_{ther} = \dot{E}_{ma,out} - \dot{E}_{ma,inl} = \dot{m} c_{p,air} \Delta T_{air} \quad (4)$$

The electrical power of the PV/T can be determined from:

$$\dot{E}_{elec} = V_{OC} I_{SC} FF \quad (5)$$

In Equation (5), FF represents a factor associated with the PV module and can be expressed mathematically as shown below [43]:

$$FF = \frac{I_{max} V_{max}}{V_{OC} I_{SC}} \quad (6)$$

The overall energy obtained from the PV/T system comprises the sum of thermal and electrical energies:

$$\dot{E}_{out} = \dot{E}_{ther} + \dot{E}_{elec} \quad (7)$$

The thermal efficiency of the PV/T system can be given as [44,45]:

$$\eta_{ther} = \frac{\dot{E}_{ma,out} - \dot{E}_{ma,in}}{\dot{E}_{sun}} \quad (8)$$

The electrical efficiency of the system can be expressed as below:

$$\eta_{elec} = \frac{\dot{E}_{elec}}{\dot{E}_{sun}} = \frac{V_{OC} I_{SC} F}{\tau \alpha \dot{G}} \quad (9)$$

General exergetic expressions for a PV/T air heating system can be given as follows:

$$\sum \dot{E}x_{in} - \sum \dot{E}x_{loss} = \sum \dot{E}x_{out} \quad (10)$$

$$\dot{E}x_{ma,in} + \dot{E}x_{sun} = \sum \dot{E}x_{dest} + \dot{E}x_{elec} + \dot{E}x_{ma,out} \quad (11)$$

The inflow exergy rate from the sun can be expressed as [46]:

$$\dot{E}x_{sun} = \dot{G} \left(1 - \frac{T_{amb}}{T_{sun}} \right) \quad (12)$$

The exergy of the mass flow rate can be represented as follows:

$$\Delta \dot{E}x_{ma} = \dot{E}x_{ma,out} - \dot{E}x_{ma,in} = \dot{m}_{air} (\phi_{out} - \phi_{in}) \quad (13)$$

Inlet and outlet flow exergies can be expressed using Equations (14) and (15), respectively:

$$\phi_{in} = (h_{in} - h_{amb}) - T_{amb}(s_{in} - s_{amb}) \quad (14)$$

$$\phi_{out} = (h_{out} - h_{amb}) - T_{amb}(s_{out} - s_{amb}) \quad (15)$$

The expressions above use the specific enthalpy (h) and specific entropy (s) notations. Additionally, there is an equation proposed by Chow et al. [47] for the electrical exergy of PV/Ts, which can be expressed as follows:

$$\dot{E}x_{elec} = \dot{E}_{elec} \quad (16)$$

The total exergy of a PV/T air heater can be expressed as:

$$\dot{E}x_{overall} = \dot{E}x_{ther} + \dot{E}x_{elec} \quad (17)$$

Electrical exergetic yield can be given as [48]:

$$\epsilon_{elec} = \frac{\dot{E}x_{elec}}{\dot{E}x_{sun}} = \frac{\dot{E}_{elec}}{\dot{G}\left(1 - \frac{T_{amb}}{T_{sun}}\right)} = \frac{V_{OC}I_{SC}FF}{\dot{G}\left(1 - \frac{T_{amb}}{T_{sun}}\right)} \quad (18)$$

The efficiency of the normalized power output is determined by comparing the output electric power achieved under actual conditions to the output obtained under standard test conditions. This efficiency can be calculated as follows [49]:

$$\eta_{npo} = \left(\frac{P_{meas}}{P_{STC}}\right) 100 \quad (19)$$

In addition, thermal exergetic yield could be calculated using Equation (20):

$$\epsilon_{ther} = \frac{\dot{E}x_{ther}}{\dot{E}x_{sun}} = \frac{\dot{m}c_{p,air} \left[(T_{air,out} - T_{air,in}) - T_{ab} \ln\left(\frac{T_{air,out}}{T_{air,in}}\right) \right]}{\dot{G}\left(1 - \frac{T_{amb}}{T_{sun}}\right)} \quad (20)$$

Total exergetic yield is the sum of thermal and electrical exergetic efficiencies:

$$\epsilon_{overall} = \epsilon_{elec} + \epsilon_{ther} \quad (21)$$

The sustainability index of a PV/T system can be determined as [50]:

$$SI = \frac{1}{1 - \epsilon_{overall}} \quad (22)$$

The expression of the experimental uncertainty is then [51]:

$$w_F = \left[\left(\frac{\partial F}{\partial x_1} w_1\right)^2 + \left(\frac{\partial F}{\partial x_2} w_2\right)^2 + \left(\frac{\partial F}{\partial x_3} w_3\right)^2 \dots + \left(\frac{\partial F}{\partial x_n} w_n\right)^2 \right]^{1/2} \quad (23)$$

The obtained average errors (uncertainties) for air temperature, air velocity, solar radiation, and thermal efficiency are ± 0.58 °C, ± 0.46 m/s, ± 17.02 W/m², and $\pm 1.78\%$, respectively. The obtained uncertainty values align well with previous studies that investigated various solar energy-based thermal systems in the academic literature, as demonstrated by Khanlari et al. [52], Alic et al. [53], and Aytacı et al. [54].

An enviro-economic investigation was performed within the scope of this research. The cost of manufacturing the system can be determined by adding up the costs of its

components. In addition, the PV/T, PV/T-TESS, and PV/T-MTESS have capital costs of 98.8 USD, 109.15 USD, and 115.80 USD, respectively.

Capital recovery factor could be determined as:

$$CF = \frac{i(1+i)^n}{(1+i)^n - 1} \quad (24)$$

In the calculations, the interest rate and life of the PV/T were considered as 0.01 and 20 years, respectively [55].

The yearly cost of the PV/T system can be found using Equation (25):

$$AC = \frac{CC}{\frac{1}{i} \left[1 - \left(\frac{1}{1+i} \right)^n \right]} \quad (25)$$

The levelized cost of heating is commonly used to evaluate the economic viability of solar-thermal systems. It is defined by the following expression, as proposed by Abuşka and Şevik [55]:

$$LCOH = \frac{CC + CF + AMC}{E_{useful}} \quad (26)$$

The acronym AMC stands for annual maintenance cost, which is assumed to be 2% of the capital cost of the PV/T.

The payback time of the PV/T is a measure used to assess the economic viability of the system. It indicates the duration required for the total investment to be repaid by the cumulative savings and can be calculated as:

$$PBT = \frac{CC}{FDS + \varphi_{CO_2}} \quad (27)$$

Here, FDS represents fuel depletion savings, which can be found using Equation (28):

$$FDS = \frac{E_{useful,overall}}{\eta_{overall}} \quad (28)$$

Annual CO_2 savings from the use of a PV/T system can be found using Equation (29):

$$\varphi_{CO_2} = \frac{\psi_{CO_2} (E_{useful,overall})}{1000} \quad (29)$$

The value of 2.08 kg CO_2 /kWh is used for ψ_{CO_2} , which corresponds to the average CO_2 emission during the generation of power using coal, according to Tripathi et al. [56].

4. Results and Discussion

As mentioned earlier, the developed PV/T air heaters were tested under identical environmental conditions to allow for a valid comparison between the different modifications. Figure 6 shows the time-dependent changes in the environmental conditions during the experiments. The measured solar radiation values ranged from 272 to 930 W/m², with an average value of 682 W/m². The ambient temperature during testing ranged from 28.9 to 33.8 °C, with an average value of 31.93 °C.

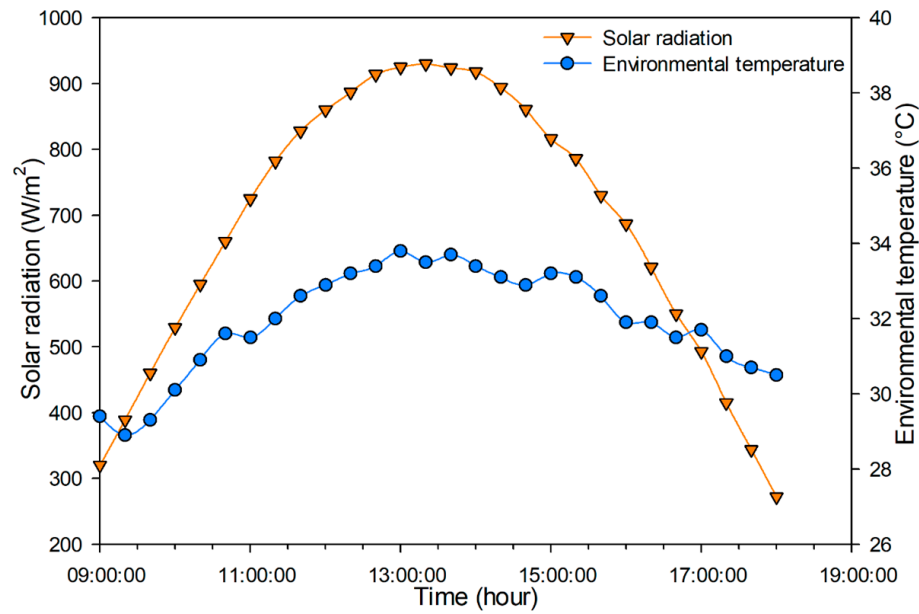


Figure 6. Time-dependent changes in environmental conditions.

The time-dependent changes in outlet air temperature values of the PV/T air heaters are presented in Figure 7. The mean outlet air temperature values for the PV/T, PV/T-TESS, and PV/T-MTESS were measured as 34.90 °C, 35.35 °C, and 35.89 °C, respectively. At 13:00, the temperature of the outlet air from PV/T-MTESS reached its highest value of 40 °C. It should be noted that the utilization of a TESS with mesh layers improved the average outlet air temperature by 2.83% compared to the unmodified PV/T configuration. Using mesh layers as extended heat transfer surfaces in the TESS led to improvements in the conductivity of the PCM and removed the heat from the PV panel surface. Similar findings were obtained in a study performed by Farzan et al. [41], which analyzed the effect of integrating mesh layers in a TESS of a solar air heating system.

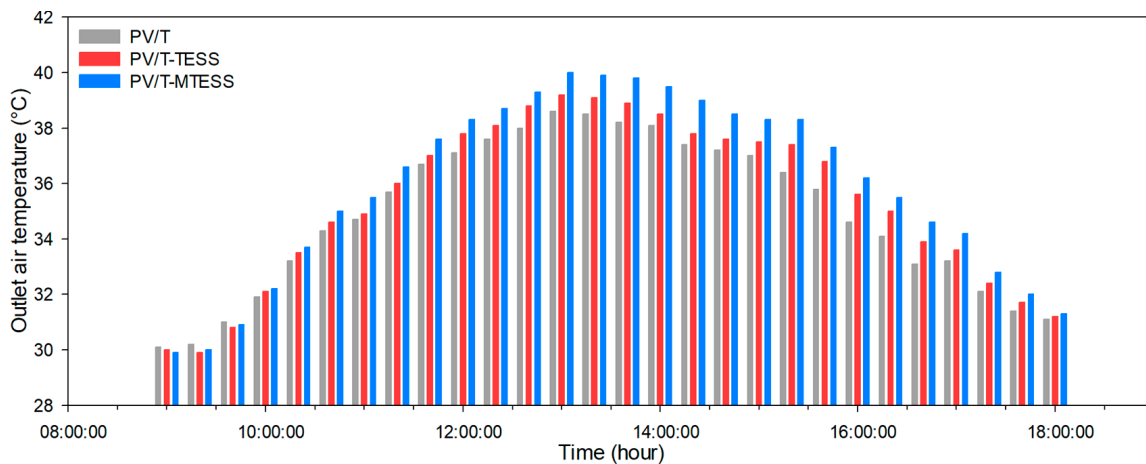


Figure 7. Time-dependent changes in outlet air temperatures.

The variations in useful thermal energy and electric power over time are displayed in Figure 8. The useful thermal energy rates for the PV/T, PV/T-TESS, and PV/T-MTESS systems were observed to be between 6.07–50.16 W, 6.10–56.18 W, and 5.08–64.21 W, respectively. The mean values of the thermal energy captured for the PV/T, PV/T-TESS, and PV/T-MTESS were 29.83 W, 34.29 W, and 39.75 W, respectively. Furthermore, the electrical power values for the PV/T, PV/T-TESS, and PV/T-MTESS were recorded as 5.34 W, 5.63 W, and 6.07 W, respectively. As the results show, using a TESS with metallic mesh layers

improved the average electric power and captured thermal energy values by 13.67% and 33.25%, respectively, compared to the unmodified PV/T air heater.

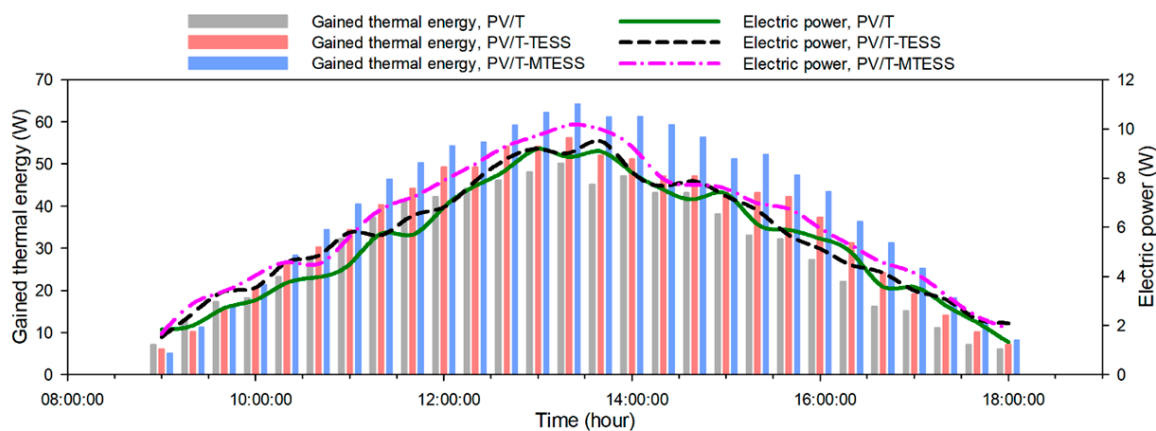


Figure 8. Time-dependent changes in electric power and gained useful thermal energy values.

Figures 9 and 10 display the recorded changes in the efficiency of the tested systems, with one graph showing thermal efficiency and the other depicting electrical efficiency. Thermal efficiency values ranged from 23.76% to 57.63% for the PV/T, 20.36% to 64.66% for the PV/T-TESS, and 16.97% to 73.77% for the PV/T-MTESS. The mean values of thermal efficiency were 43.62%, 50.10%, and 58.09% for the PV/T, PV/T-TESS, and PV/T-MTESS, respectively. While the average electrical efficiencies were 7.96%, 8.49%, and 9.14% for the PV/T, PV/T-TESS, and PV/T-MTESS, respectively. The addition of a paraffin-containing TESS resulted in a 14.85% improvement in average thermal efficiency and a 6.65% improvement in average electrical efficiency. Additionally, the incorporation of mesh layers in the TESS improved the average values of the thermal and electrical efficiencies by 33.17% and 14.82%, respectively, compared to the conventional PV/T configuration. It should be noted that overall efficiency values, which are the sum of thermal and electrical efficiencies, for the PV/T, PV/T-TESS, and PV/T-MTESS systems were 51.58%, 58.59%, and 67.22%, respectively. Employing a TESS with mesh layers in the conventional system improved the overall efficiency by 30.32%. Moreover, it can be clearly seen from Figure 9, integrating steel mesh into the system reduced the discharging time of the used PCM. As can be seen in the thermal efficiency graph, at the beginning of the experimental period, the efficiency of the unmodified system is high in comparison with other systems. The main reason for this is that the thermal energy is used for heating the PCM in the modified systems. In other words, after melting the PCM, the temperature distribution becomes more homogeneous in the modified systems. After that, the thermal efficiency values of the modified systems reach higher values in comparison with the unmodified system. An increment in thermal yield occurred in both PV/T systems with TESS but the PCM in the mesh-integrated system (PV/T-MTESS) started to discharge earlier than the PV/T with a paraffin-only TESS. Moreover, similar behaviors in electrical and thermal yields were obtained in some literature studies. In a study conducted by Ahmadi et al. [57], PCM-based composites were utilized to enhance the performance of a PV/T system, which resulted in an electrical efficiency improvement of 14%, a rate very similar to the improvement seen in the present work. In their analysis of a novel PV/T system utilizing a PCM-based heat exchanger, Diallo et al. [58] discovered that implementing new modifications resulted in a significant enhancement of the system's overall efficiency by 28%. In another experimental study, Choubineh et al. [59] developed a PV/T air heating system with PCMs and improved the electrical efficiency value by 9%. It is worth noting that the overall efficiency values obtained in this study are in good agreement with similar works that have analyzed different types of PV/T air system configurations [60–63].

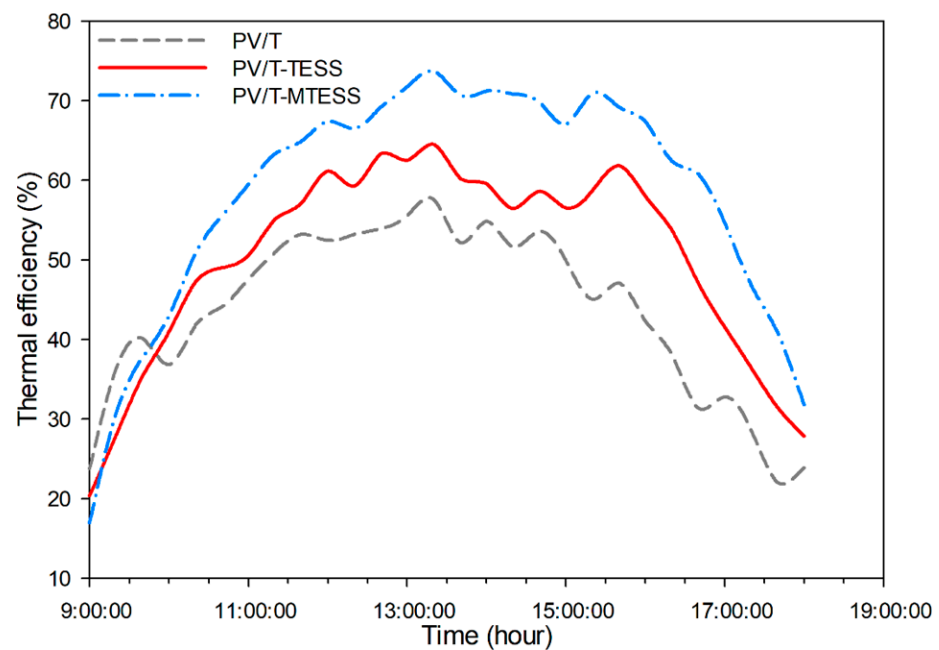


Figure 9. Time-dependent changes in thermal efficiency values.

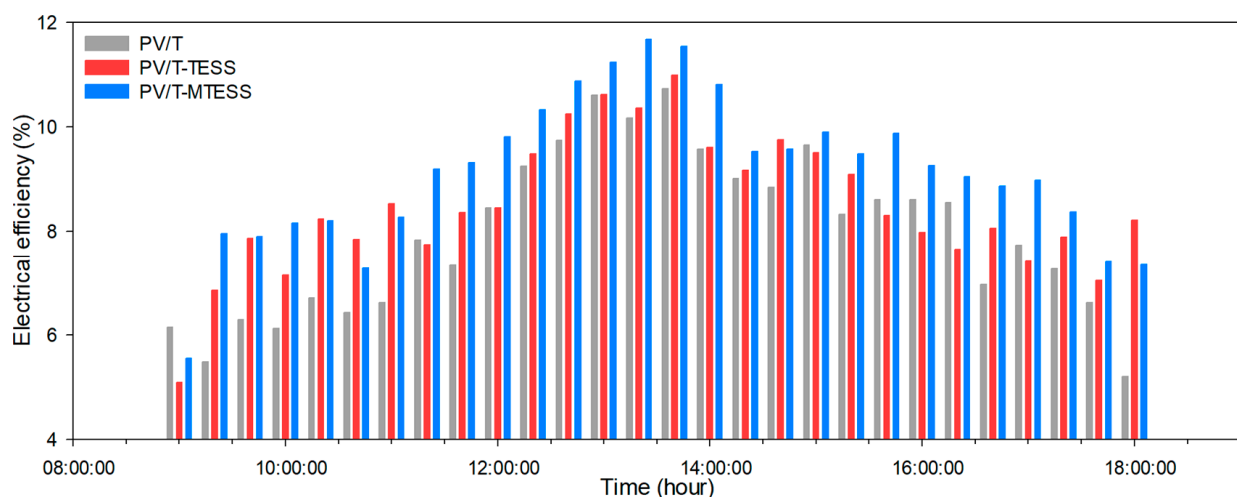


Figure 10. Time-dependent changes in electrical efficiency values.

Figure 11 shows the time-dependent changes in the overall exergetic efficiencies of the analyzed systems. The total exergetic efficiencies, which were the sum of thermal and electrical exergetic efficiencies, for the PV/T, PV/T-TESS, and PV/T-MTESS were found to be 2.82%, 3.51%, and 4.46%, respectively. The use of TESSs containing paraffin and mesh layer-integrated paraffin improved the mean total exergetic efficiency values by 24.46% and 58.15%, respectively. In a previous study, Abdelkader et al. [64] reported average exergetic efficiency values between 1.92% to 2.77% for a solar air heating system. Similarly, Mugi and Chandramohan [50] determined the average exergetic efficiency of a solar energy-based air heating system, which ranged from 0.33% to 4.06%. Nayak and Tiwari [65] tested a PV/T system and reported an overall exergy efficiency of approximately 4%.

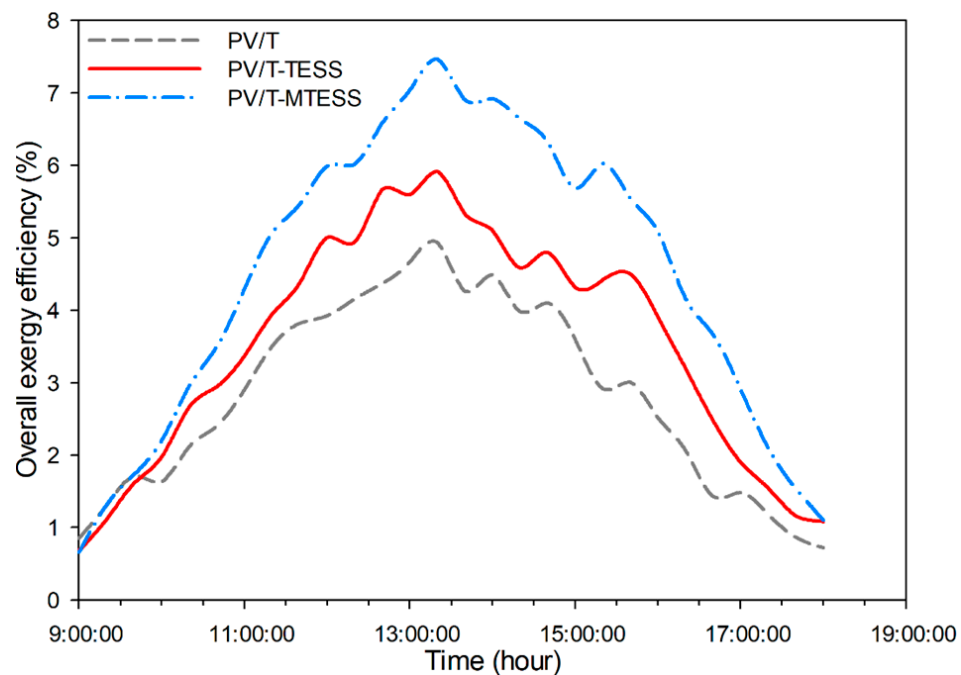


Figure 11. Time-dependent changes in total exergetic efficiencies.

Figure 12 shows the time-dependent changes in the normalized power output efficiencies, which is a widely used parameter in PV systems. This ratio signifies the power measurement obtained under real-world operating conditions compared to those recorded during standard testing conditions. The average normalized power output efficiencies for the PV/T, PV/T-TESS, and PV/T-MTESS were found to be 44.50%, 46.88%, and 50.59%, respectively. In addition, the instantaneous values of this parameter for the PV/T, PV/T-TESS, and PV/T-MTESS ranged between 11.03–77.39%, 12.68–79.26%, and 13.83–84.67%, respectively, during the experimental analysis. The use of a mesh layer-integrated TESS in the system improved the normalized power output efficiency of the conventional configuration by 13.68%. Wongwuttanasatian et al. [66] conducted a study where they utilized heat sinks and TESSs to enhance the efficiency of PV panels. Similar to our work, the implementation of these modifications led to an improvement in the normalized power output efficiency value.

The results presented in Figure 13 indicate that the use of a mesh layer-embedded TESS in the PV/T system has improved both the electrical exergy and thermal exergy efficiencies, as well as the sustainability index, and reduced the payback time. Specifically, the enhancement in thermal exergy efficiency was significant, with a 73.55% increase compared to the conventional system. The sustainability index values for all tested systems were found to be between 1.0292–1.0471, indicating that the systems are environmentally sustainable. In terms of payback time, the PV/T-MTESS had the shortest payback time of 1.117 years, indicating that the system is economically feasible. This is a significant reduction in payback time compared to some previous studies, where payback times were found to be between 1.9–2.1 years for different configurations [67]. Daghigh et al. [68] conducted an investigation of a PV/T system and determined a payback period ranging from 2.3 to 2.5 years. The current study also revealed that the average LCOH values for PV/T, PV/T-TESS, and PV/T-MTESS systems were 0.0386, 0.0376, and 0.0347 USD/kWh, respectively. These values were lower than the LCOH value reported in a previous study [69] on a PV/T-assisted heating system, for which the LCOH value was found to be 0.054 USD/kWh. This suggests that the use of TESSs, particularly mesh layer-embedded TESSs, can lead to a more cost-effective and sustainable energy solution.

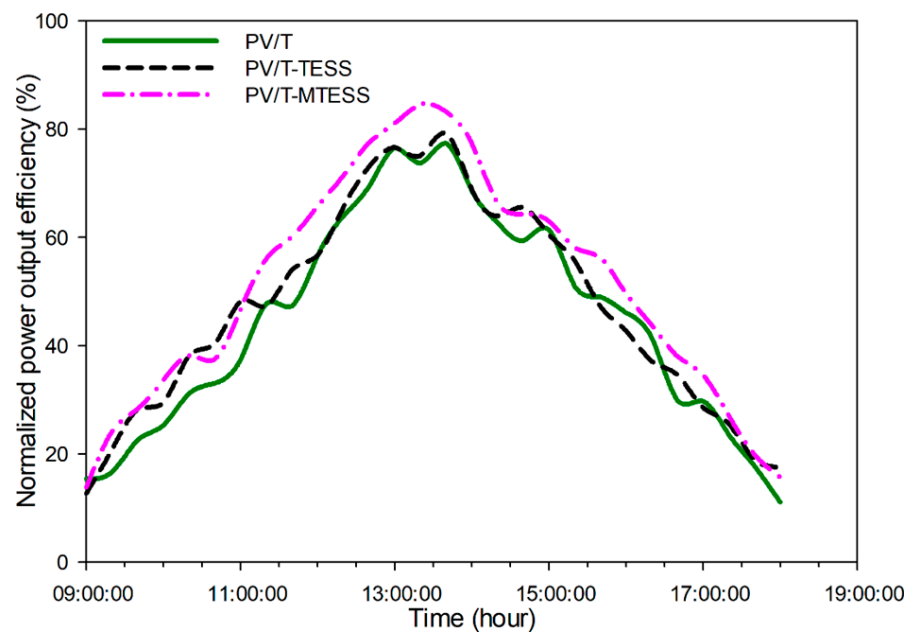


Figure 12. Time-dependent changes in normalized power output efficiencies.

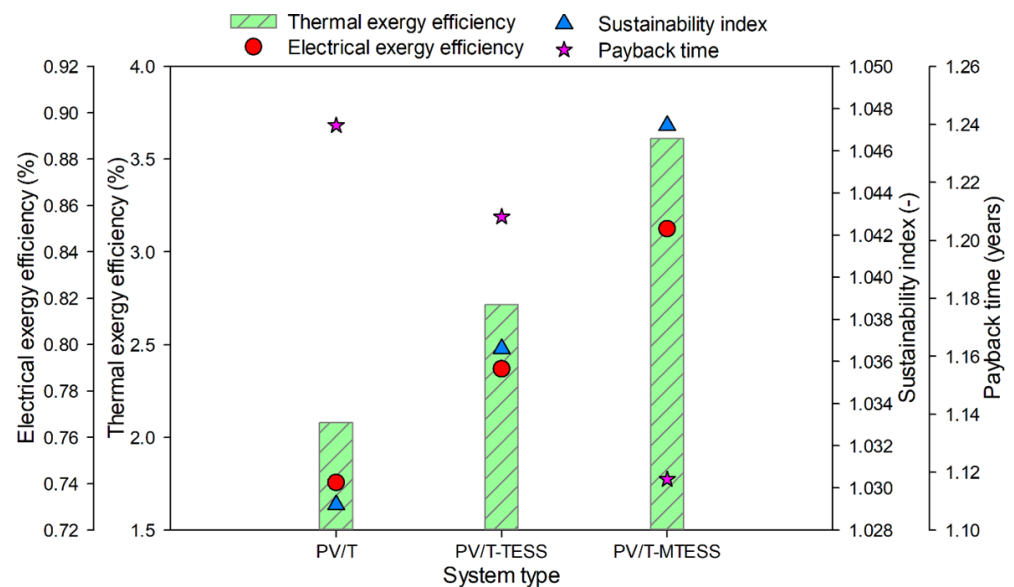


Figure 13. Obtained average performance indicators.

In another study, a hybrid PV/T system has been analyzed and this parameter was found between the range of 0.012–0.014 USD/kWh [70]. Carbon dioxide saving values were also calculated as an important performance indicator. Annual carbon dioxide savings for the PV/T, PV/T-TESS, and PV/T-MTESS were obtained as 0.079, 0.090, and 0.103 tons/year, respectively. As can be seen, using the TESS with mesh layers improved the annual carbon dioxide savings of the conventional PV/T system by 30.37%. In a similar study, a hybrid solar system has been developed and yearly carbon dioxide savings were obtained of between 0.4 and 2.7 tons/year [71]. In another study, Abuşka and Şevik [55] designed and analyzed various types of solar air heating systems and obtained yearly CO₂ savings in the range of 0.31 to 0.40 tons/year. The enviro-economic performance indicators obtained in this study for the analyzed PV/T air heaters are consistent with those reported in other academic literature, suggesting a reliable outcome.

The main aim of this work is to investigate the effect of adding mesh layers into the PCM-filled container on the overall performance of a PV/T system. In this regard, an

unmodified PV/T, a PV/T equipped with a PCM container, and a PV/T with a mesh-integrated PCM container were developed and experimentally analyzed. PCM-integrated PV/T systems presented a higher thermal performance than an unmodified system in terms of extending the utilization time period of the system. In addition, adding mesh layers had positive effects on the melting process of the PCM and consequently, the overall thermal performance of the modified system. It can be said that the effect of adding a PCM-filled container on the utilization period of the system is greater than that of decreasing the surface temperature of the PV module.

5. Conclusions

This study focuses on enhancing the thermal and electrical performance of a PV/T air heating system through the use of a metallic mesh-embedded TESS. To achieve this goal, three PV/T air heaters were designed, manufactured, and experimentally evaluated. The key findings of this work are:

- Employing a TESS with metallic mesh layers improved average electric power and gained thermal energy values by 13.67% and 33.25%, respectively, in comparison to the unmodified PV/T air heater.
- Using only a paraffin-containing TESS upgraded the mean thermal and electrical yields by 14.85% and 6.65%, respectively. By adding mesh layers to the TESS, there was a significant enhancement in the overall performance of the PV/T system, with thermal and electrical efficiencies surpassing the values achieved by the unmodified system by 33.17% and 14.82%, respectively.
- The average LCOH value of the unmodified system was reduced from 0.0386 USD/kWh to 0.0347 USD/kWh using a metallic mesh layer-embedded TESS.
- Utilizing the TESS with mesh layers enhanced the yearly carbon dioxide savings by 30.37% compared to the unmodified PV/T air heater.

The results obtained from this study demonstrate the beneficial effects of incorporating metallic mesh layers into the TESS of a pilot-scale PV/T air heating system. These results can serve as a reference for conducting research on larger-scale PV/T air heating systems. The study also demonstrated improvements in both cases where paraffin was used alone and where paraffin was combined with mesh layers. Therefore, future studies can test different numbers of mesh layers to assess their impact on system performance. Moreover, different optimization techniques can be applied to the experimental data to determine the best configuration.

Author Contributions: Conceptualization, A.D.T.; methodology, A.D.T. and E.Y.G.; validation, A.D.T., E.Y.G. and A.K.; investigation, A.D.T. and A.G.G.; writing—original draft preparation, A.D.T. and E.Y.G.; writing—review and editing, A.D.T., E.Y.G., A.K. and A.G.G.; visualization, A.D.T.; supervision, A.G.G. All authors have read and agreed to the published version of the manuscript.

Funding: This research received no external funding.

Institutional Review Board Statement: Not applicable.

Informed Consent Statement: Not applicable.

Data Availability Statement: Not applicable.

Conflicts of Interest: The authors declare no conflict of interest.

Nomenclature

A	surface area of the PV/T, m^2
c_p	specific heat capacity of the air, kJ/kgK
CC	capital cost of the PV/T system, USD
CF	capital recovery factor, -

\dot{E}	energy rate, W
\dot{E}_x	exergy rate, W
FDS	fuel depletion savings, USD
FF	fill factor of the PV panel, -
\dot{G}	solar irradiation, W/m ²
\dot{G}_{ef}	effective solar radiation, W
h	enthalpy, kJ/kg
I	electric current, A
LCOH	levelized cost of heating, USD/kWh
m	mass, kg
\dot{m}	mass flow rate of air in the PV/T, kg/s
P	electric power, W
PBT	payback time of the PV/T, year
s	entropy, kJ/kgK
SI	sustainability index, -
T	temperature, K
V	electric voltage, V
Greek symbols	
α	absorptivity, -
ΔT	temperature difference, K
τ	transmissivity, -
η	efficiency, %
ϕ	flow exergy, -
φ_{CO_2}	yearly CO ₂ savings, tons/year
ψ_{CO_2}	average CO ₂ emission for power production by coal, kgCO ₂ /kWh
Subscripts	
<i>dest</i>	destroyed
<i>elec</i>	electrical
<i>ef</i>	effective
<i>exg</i>	exergy
<i>in</i>	inlet
<i>ma</i>	air mass
<i>meas</i>	measured
<i>npo</i>	normalized power output
<i>OC</i>	open circuit
<i>out</i>	outlet
<i>SC</i>	short circuit
<i>STC</i>	Standard Test Conditions
<i>ther</i>	thermal

References

- Farzan, H.; Zaim, E.H.; Ameri, M.; Amiri, T. Study on effects of wind velocity on thermal efficiency and heat dynamics of pavement solar collectors: An experimental and numerical study. *Renew. Energy* **2021**, *163*, 1718–1728. [[CrossRef](#)]
- Khanlari, A.; Tuncer, A.D.; Sözen, A.; Aytac, İ.; Çiftçi, E.; Variyenli, H.İ. Energy and exergy analysis of a vertical solar air heater with nano-enhanced absorber coating and perforated baffles. *Renew. Energy* **2022**, *187*, 586–602. [[CrossRef](#)]
- Farzan, H.; Zaim, E.H. Study on thermal performance of a new combined perforated metallic/asphalt solar air heater for heating Applications: An experimental study. *Sol. Energy* **2023**, *249*, 485–494. [[CrossRef](#)]
- Nižetić, S.; Jurčević, M.; Čoko, D.; Arıcı, M. A novel and effective passive cooling strategy for photovoltaic panel. *Renew. Sustain. Energy Rev.* **2021**, *145*, 111164. [[CrossRef](#)]
- Tuncer, A.D.; Khanlari, A.; Sözen, A. Seasonal energy-exergy analysis of a new foldable photovoltaic-thermal air collector: An experimental and numerical study. *Heat Transf. Res.* **2022**, *53*, 25–53. [[CrossRef](#)]
- Azad, A.K.; Parvin, S. Bibliometric analysis of photovoltaic thermal (PV/T) system: From citation mapping to research agenda. *Energy Rep.* **2022**, *8*, 2699–2711. [[CrossRef](#)]
- Vengadesan, E.; Senthil, R. A review on recent developments in thermal performance enhancement methods of flat plate solar air collector. *Renew. Sustain. Energy Rev.* **2020**, *134*, 110315. [[CrossRef](#)]
- Jamshed, W.; Şirin, C.; Selimefendigil, F.; Shamsuddin, M.D.; Altowairqi, Y.; Eid, M.R. Thermal characterization of coolant Maxwell type nanofluid flowing in Parabolic Trough Solar Collector (PTSC) used inside solar powered ship application. *Coatings* **2021**, *11*, 1552. [[CrossRef](#)]

9. Khadiran, T.; Hussein, M.Z.; Zainal, Z.; Rusli, R. Advanced energy storage materials for building applications and their thermal performance characterization: A review. *Renew. Sustain. Energy Rev.* **2016**, *57*, 916–928. [[CrossRef](#)]
10. Bayrak, F.; Oztop, H.F.; Selimefendigil, F. Effects of different fin parameters on temperature and efficiency for cooling of photovoltaic panels under natural convection. *Sol. Energy* **2019**, *188*, 484–494. [[CrossRef](#)]
11. Herrando, M.; Ramos, A. Photovoltaic-Thermal (PV-T) systems for combined cooling, heating and power in buildings: A review. *Energies* **2022**, *15*, 3021. [[CrossRef](#)]
12. Kumar, R.; Rosen, M.A. Performance evaluation of a double pass PV/T solar air heater with and without fins. *Appl. Therm. Eng.* **2011**, *31*, 1402–1410. [[CrossRef](#)]
13. Othman, M.Y.; Hamid, S.A.; Tabook, M.A.S.; Sopian, K.; Roslan, M.H.; Ibarahim, Z. Performance analysis of PV/T combi with water and air heating system: An experimental study. *Renew. Energy* **2016**, *86*, 716–722. [[CrossRef](#)]
14. Mourshed, M.; Masuk, N.I.; Nguyen, H.Q.; Shabani, B. An experimental approach to energy and exergy analyses of a hybrid PV/T system with simultaneous water and air cooling. *Energies* **2022**, *15*, 6764. [[CrossRef](#)]
15. Vassiliades, C.; Barone, G.; Buonomano, A.; Forzano, C.; Giuzio, G.F.; Palombo, A. Assessment of an innovative plug and play PV/T system integrated in a prefabricated house unit: Active and passive behaviour and life cycle cost analysis. *Renew. Energy* **2022**, *186*, 845–863. [[CrossRef](#)]
16. Kang, Z.; Lu, Z.; Song, G.; Yao, Q. A numerical study of dual-inlet air-cooled PV/T solar collectors with various airflow channel configurations. *Sustainability* **2022**, *14*, 9897. [[CrossRef](#)]
17. Gopi, S.; Muraleedharan, C. Modelling and experimental studies on a double-pass hybrid photovoltaic-thermal solar air heater with vertical slats attached in the lower channel. *Int. J. Amb. Energy* **2022**, *43*, 4664–4674. [[CrossRef](#)]
18. Shahsavari, A.; Arıcı, M. Energy and exergy analysis and optimization of a novel heating, cooling, and electricity generation system composed of PV/T-heat pipe system and thermal wheel. *Renew. Energy* **2023**, *203*, 394–406. [[CrossRef](#)]
19. Roshdan, W.N.A.W.; Jarimi, H.; Al-Waeli, A.H.; Ramadan, O.; Sopian, K. Performance enhancement of double pass photovoltaic/thermal solar collector using asymmetric compound parabolic concentrator (PV/T-ACPC) for façade application in different climates. *Case Stud. Therm. Eng.* **2022**, *34*, 101998. [[CrossRef](#)]
20. Farzan, H.; Zaim, E.H.; Amiri, T. Performance study on a new solar air heater with integrated phase change materials and external recycle: A numerical and experimental study. *Appl. Therm. Eng.* **2023**, *223*, 120000. [[CrossRef](#)]
21. Selimefendigil, F.; Şirin, C. Energy and exergy analysis of a hybrid photovoltaic/thermal-air collector modified with nano-enhanced latent heat thermal energy storage unit. *J. Energy Storage* **2022**, *45*, 103467. [[CrossRef](#)]
22. Gürbüz, E.Y.; Kusun, B.; Tuncer, A.D.; Ural, T. Experimental investigation of a double-flow photovoltaic/thermal air collector with natural dolomite powder-embedded thermal energy storage unit. *J. Energy Storage* **2023**, *64*, 107220. [[CrossRef](#)]
23. Şirin, C.; Selimefendigil, F.; Özttop, H.F. Performance analysis and identification of an indirect photovoltaic thermal dryer with aluminum oxide nano-embedded thermal energy storage modification. *Sustainability* **2023**, *15*, 2422. [[CrossRef](#)]
24. Selimefendigil, F.; Şirin, C.; Ghachem, K.; Kolsi, L. Exergy and environmental analysis of an active greenhouse dryer with Al₂O₃ nano-embedded latent heat thermal storage system: An experimental study. *Appl. Therm. Eng.* **2022**, *217*, 119167. [[CrossRef](#)]
25. Selimefendigil, F.; Şirin, C.; Özttop, H.F. Experimental analysis of combined utilization of CuO nanoparticles in latent heat storage unit and absorber coating in a single-slope solar desalination system. *Sol. Energy* **2022**, *233*, 278–286. [[CrossRef](#)]
26. Browne, M.C.; Quigley, D.; Hard, H.R.; Gilligan, S.; Ribeiro, N.C.; Almeida, N.; McCormack, S.J. Assessing the thermal performance of phase change material in a photovoltaic/thermal system. *Energy Procedia* **2016**, *91*, 113–121. [[CrossRef](#)]
27. Yang, X.; Sun, L.; Yuan, Y.; Zhao, X.; Cao, X. Experimental investigation on performance comparison of PV/T-PCM system and PV/T system. *Renew. Energy* **2018**, *119*, 152–159. [[CrossRef](#)]
28. Selimefendigil, F.; Şirin, C.; Özttop, H.F. Effect of different heat transfer fluids on discharging performance of phase change material included cylindrical container during forced convection. *J. Cent. South Univ.* **2021**, *28*, 3521–3533. [[CrossRef](#)]
29. Sopian, K.; Al-Waeli, A.H.; Kazem, H.A. Energy, exergy and efficiency of four photovoltaic thermal collectors with different energy storage material. *J. Energy Storage* **2020**, *29*, 101245. [[CrossRef](#)]
30. Behzadi, A.; Arabkoohsar, A. Feasibility study of a smart building energy system comprising solar PV/T panels and a heat storage unit. *Energy* **2020**, *210*, 118528. [[CrossRef](#)]
31. Yao, J.; Xu, H.; Dai, Y.; Huang, M. Performance analysis of solar assisted heat pump coupled with build-in PCM heat storage based on PV/T panel. *Sol. Energy* **2020**, *197*, 279–291. [[CrossRef](#)]
32. Mao, Y.; Wu, J.; Zhang, W. An effective operation strategy for CCHP system integrated with photovoltaic/thermal panels and thermal energy storage. *Energies* **2020**, *13*, 6418. [[CrossRef](#)]
33. Gulfam, R.; Zhang, P.; Meng, Z. Advanced thermal systems driven by paraffin-based phase change materials—A review. *Appl. Energy* **2019**, *238*, 582–611. [[CrossRef](#)]
34. Wei, G.; Wang, G.; Xu, C.; Ju, X.; Xing, L.; Du, X.; Yang, Y. Selection principles and thermophysical properties of high temperature phase change materials for thermal energy storage: A review. *Renew. Sustain. Energy Rev.* **2018**, *81*, 1771–1786. [[CrossRef](#)]
35. Yang, L.; Huang, J.; Zhou, F. Thermophysical properties and applications of nano-enhanced PCMs: An update review. *Energy Convers. Manag.* **2020**, *214*, 112876. [[CrossRef](#)]
36. Kabeel, A.E.; Khalil, A.; Shalaby, S.M.; Zayed, M.E. Experimental investigation of thermal performance of flat and v-corrugated plate solar air heaters with and without PCM as thermal energy storage. *Energy Convers. Manag.* **2016**, *113*, 264–272. [[CrossRef](#)]

37. Sajawal, M.; Rehman, T.U.; Ali, H.M.; Sajjad, U.; Raza, A.; Bhatti, M.S. Experimental thermal performance analysis of finned tube-phase change material based double pass solar air heater. *Case Stud. Therm. Eng.* **2019**, *15*, 100543. [[CrossRef](#)]
38. Salih, S.M.; Jalil, J.M.; Najim, S.E. Experimental and numerical analysis of double-pass solar air heater utilizing multiple capsules PCM. *Renew. Energy* **2019**, *143*, 1053–1066. [[CrossRef](#)]
39. Abuşka, M.; Şevik, S.; Kayapınar, A. A comparative investigation of the effect of honeycomb core on the latent heat storage with PCM in solar air heater. *Appl. Therm. Eng.* **2019**, *148*, 684–693. [[CrossRef](#)]
40. Dinesh, S.N.; Saminathan, R.; Patil, M.M.; Baviskar, P.R.; Hadidi, H.; Vignesh, S.; Kumar, P.M. Investigating the single pass baffled solar air heater (SAH) with an organic PCM (OPCM). *Mater. Today Proceed.* **2022**, *62*, 5245–5249. [[CrossRef](#)]
41. Farzan, H.; Zaim, E.H.; Amiri, T. Performance investigation on a new solar air heater using phase change material/expanded metal mesh composite as heat storage unit: An experimental study. *J. Energy Storage* **2022**, *47*, 103602. [[CrossRef](#)]
42. Kazemian, A.; Taheri, A.; Sardarabadi, A.; Ma, T.; Passandideh-Fard, M.; Peng, J. Energy, exergy and environmental analysis of glazed and unglazed PVT system integrated with phase change material: An experimental approach. *Sol. Energy* **2020**, *201*, 178–189. [[CrossRef](#)]
43. Granstrom, M.; Petritsch, K.; Arias, A.C.; Lux, A.; Andersson, M.R.; Friend, R.H. Laminated fabrication of polymeric photovoltaic diodes. *Nature* **1998**, *395*, 257–260. [[CrossRef](#)]
44. Khanlari, A.; Tuncer, A.D.; Afshari, F.; Sözen, G. Utilization of recyclable aluminum cans as fins in a vertical solar air heating system: An experimental and numerical study. *J. Build. Eng.* **2023**, *63*, 105446. [[CrossRef](#)]
45. Selimefendigil, F.; Şirin, C.; Ghachem, K.; Kolsi, L.; Alqahtani, T.; Algarni, S. Enhancing the performance of a greenhouse drying system by using triple-flow solar air collector with nano-enhanced absorber coating. *Case Stud. Therm. Eng.* **2022**, *34*, 102011. [[CrossRef](#)]
46. Park, S.R.; Pandey, A.K.; Tyagi, V.V.; Tyagi, S.K. Energy and exergy analysis of typical renewable energy systems. *Renew. Sustain. Energy Rev.* **2014**, *30*, 105–123. [[CrossRef](#)]
47. Chow, T.T.; Pei, G.; Fong, K.F.; Lin, Z.; Chan, A.L.S.; Ji, J. Energy and exergy analysis of photovoltaic–thermal collector with and without glass cover. *Appl. Energy* **2009**, *86*, 310–316. [[CrossRef](#)]
48. Tuncer, A.D.; Khanlari, A.; Afshari, F.; Sözen, A.; Çiftçi, E.; Kusun, B.; Şahinkesen, İ. Experimental and numerical analysis of a grooved hybrid photovoltaic-thermal solar drying system. *Appl. Therm. Eng.* **2023**, *218*, 119288. [[CrossRef](#)]
49. Tuncer, A.D.; Khanlari, A.; Aytac, İ.; Çiftçi, E.; Sözen, A.; Variyenli, H.İ. Passive thermal management of photovoltaic panel by using phase change material-filled aluminum cans: An experimental study. *Heat Transf. Res.* **2022**, *53*, 72–86. [[CrossRef](#)]
50. Mugi, V.R.; Chandramohan, V.P. Energy and exergy analysis of forced and natural convection indirect solar dryers: Estimation of exergy inflow, outflow, losses, exergy efficiencies and sustainability indicators from drying experiments. *J. Clean. Prod.* **2021**, *282*, 124421. [[CrossRef](#)]
51. Variyenli, H.İ.; Amini, A.; Tuncer, A.D.; Khanlari, A.; Kolay, Ş. Experimental and numerical analysis of a helically-coiled solar water collector at various angular placements. *Int. J. Therm. Sci.* **2023**, *188*, 108177. [[CrossRef](#)]
52. Khanlari, A.; Güler, H.Ö.; Tuncer, A.D.; Şirin, C.; Bilge, Y.C.; Yılmaz, Y.; Güngör, A. Experimental and numerical study of the effect of integrating plus-shaped perforated baffles to solar air collector in drying application. *Renew. Energy* **2020**, *145*, 1677–1692. [[CrossRef](#)]
53. Alic, E.; Das, M.; Akpınar, E.K. Design, manufacturing, numerical analysis and environmental effects of single-pass forced convection solar air collector. *J. Clean. Prod.* **2021**, *311*, 127518. [[CrossRef](#)]
54. Aytac, İ.; Tuncer, A.D.; Khanlari, A.; Variyenli, H.İ.; Mantıçı, S.; Güngör, L.; Ünvar, S. Investigating the effects of using MgO-CuO/water hybrid nanofluid in an evacuated solar water collector: A comprehensive survey. *Therm. Sci. Eng. Prog.* **2023**, *39*, 101688. [[CrossRef](#)]
55. Abuşka, M.; Şevik, S. Energy, exergy, economic and environmental (4E) analyses of flat-plate and V-groove solar air collectors based on aluminium and copper. *Sol. Energy* **2017**, *158*, 259–277. [[CrossRef](#)]
56. Tripathi, R.; Tiwari, G.N.; Dwivedi, V.K. Overall energy, exergy and carbon credit analysis of N partially covered Photovoltaic Thermal (PVT) concentrating collector connected in series. *Sol. Energy* **2016**, *136*, 260–267. [[CrossRef](#)]
57. Ahmadi, R.; Monadinia, F.; Maleki, M. Passive/active photovoltaic-thermal (PVT) system implementing infiltrated phase change material (PCM) in PS-CNT foam. *Sol. Energy Mater. Sol. Cells* **2021**, *222*, 110942. [[CrossRef](#)]
58. Diallo, T.M.; Yu, M.; Zhou, J.; Zhao, X.; Shittu, S.; Li, G.; Hardy, D. Energy performance analysis of a novel solar PVT loop heat pipe employing a microchannel heat pipe evaporator and a PCM triple heat exchanger. *Energy* **2019**, *167*, 866–888. [[CrossRef](#)]
59. Choubineh, N.; Jannesari, H.; Kasaeian, A. Experimental study of the effect of using phase change materials on the performance of an air-cooled photovoltaic system. *Renew. Sustain. Energy Rev.* **2019**, *101*, 103–111. [[CrossRef](#)]
60. Agrawal, S.; Tiwari, G.N.; Pandey, H.D. Indoor experimental analysis of glazed hybrid photovoltaic thermal tiles air collector connected in series. *Energy Build.* **2012**, *53*, 145–151. [[CrossRef](#)]
61. Jahromi, S.N.; Vadiiee, A.; Yaghoubi, M. Exergy and economic evaluation of a commercially available PV/T collector for different climates in Iran. *Energy Procedia* **2015**, *75*, 444–456. [[CrossRef](#)]
62. Sarhaddi, F.; Farahat, S.; Ajam, H.; Behzadmehr, A. Exergetic performance assessment of a solar photovoltaic thermal (PV/T) air collector. *Energy Build.* **2010**, *42*, 2184–2199. [[CrossRef](#)]

63. Slimani, M.E.A.; Amirat, M.; Kurucz, I.; Bahria, S.; Hamidat, A.; Chaouch, W.B. A detailed thermal-electrical model of three photovoltaic/thermal (PV/T) hybrid air collectors and photovoltaic (PV) module: Comparative study under Algiers climatic conditions. *Energy Convers. Manag.* **2017**, *133*, 458–476. [[CrossRef](#)]
64. Abdelkader, T.K.; Zhang, Y.; Gaballah, E.S.; Wang, S.; Wan, Q.; Fan, Q. Energy and exergy analysis of a flat-plate solar air heater coated with carbon nanotubes and cupric oxide nanoparticles embedded in black paint. *J. Clean. Prod.* **2020**, *250*, 119501. [[CrossRef](#)]
65. Nayak, S.; Tiwari, G.N. Energy and exergy analysis of photovoltaic/thermal integrated with a solar greenhouse. *Energy Build.* **2008**, *40*, 2015–2021. [[CrossRef](#)]
66. Wongwuttanasatian, T.; Sarikarin, T.; Suksri, A. Performance enhancement of a photovoltaic module by passive cooling using phase change material in a finned container heat sink. *Sol. Energy* **2020**, *195*, 47–53. [[CrossRef](#)]
67. Jha, P.; Mondol, J.D.; Das, B.; Gupta, R. Energy metrics assessment of a photovoltaic thermal air collector (PVTAC): A comparison between flat and wavy collector. *Energy Sources Part A* **2020**, *42*, 1–19. [[CrossRef](#)]
68. Daghigh, R.; Shahidian, R.; Oramipoor, H. A multistate investigation of a solar dryer coupled with photovoltaic thermal collector and evacuated tube collector. *Sol. Energy* **2020**, *199*, 694–703. [[CrossRef](#)]
69. Yao, J.; Zheng, S.; Chen, D.; Dai, Y.; Huang, M. Performance improvement of vapor-injection heat pump system by employing PVT collector/evaporator for residential heating in cold climate region. *Energy* **2021**, *219*, 119636. [[CrossRef](#)]
70. Riggs, B.C.; Biedenharn, R.; Dougher, C.; Ji, Y.V.; Xu, Q.; Romanin, V.; Escarra, M.D. Techno-economic analysis of hybrid PV/T systems for process heat using electricity to subsidize the cost of heat. *Appl. Energy* **2017**, *208*, 1370–1378. [[CrossRef](#)]
71. Rekha, L.; Vijayalakshmi, M.M.; Natarajan, E. Green house saving potential of a photovoltaic thermal hybrid solar system for residential applications. *Int. J. Innov. Res. Sci. Eng. Technol.* **2013**, *2*, 370–376.

Disclaimer/Publisher's Note: The statements, opinions and data contained in all publications are solely those of the individual author(s) and contributor(s) and not of MDPI and/or the editor(s). MDPI and/or the editor(s) disclaim responsibility for any injury to people or property resulting from any ideas, methods, instructions or products referred to in the content.